SUPPLEMENTARY INFORMATION

1 Pulsation Properties

The large separation $\Delta\nu$ for each star is listed in Table S1. In most cases this was measured by aligning the high-frequency radial modes ($n = 4$ to 8) in a vertical ridge in the échelle diagram (see Fig. 1). In stars without a clear sequence of radial modes, such as those in Fig. 4, $\Delta\nu$ is less well constrained because the ridges are not quite parallel.

The phase term ϵ is given for those stars having a clear $l = 0$ sequence, as determined from the horizontal position of that ridge in the échelle diagram. Note that $\Delta\nu$ and ϵ are related to the frequencies of high-order radial modes via the asymptotic relation: $\nu_{n,l=0} \approx \Delta\nu(n + \epsilon)$.

2 Fundamental Stellar Properties

To calculate properties for our sample we used Tycho B_T and V_T photometry[1], which we transformed into Johnson B and V magnitudes[2]. We then used a $(B - V)$–$T_{\rm eff}$ relation[3], Gaia DR2 parallaxes[4], a 3D dust map[5], and V-band bolometric corrections to calculate effective temperatures and luminosities. We did this by solving for the distance modulus, as implemented in the "direct mode" version of `isoclassify`[6]. For four stars without reliable Tycho photometry ($V_T > 10$ mag) we used Gaia BP and RP magnitudes, with which we interpolated the colour–$T_{\rm eff}$ relation in the MIST (MESA Isochrones and Stellar Tracks) model grid[7] for solar metallicity to derive $T_{\rm eff}$, and used 2MASS K-band magnitudes in combination with Gaia parallaxes to derive luminosities.

We adopted 2% fractional uncertainties for all derived effective temperatures, which is typical of the residual scatter in optical colour-temperature relations[8]. Comparisons with temperatures of A-type stars in the *Kepler* Stellar Properties Catalog[9] and with an independent implementation of the infrared flux method (IRFM) both showed good agreement with no significant systematic offsets.

To estimate mean stellar densities, we fitted the effective temperatures and luminosities derived in the previous step to MIST isochrones using the "grid mode" of `isoclassify`, assuming a solar-neighborhood metallicity prior. The procedure also yielded estimates of stellar masses and surface gravities, which combined with $T_{\rm eff}$ were used for the interpolation of bolometric corrections in the previous step. We iterated between the "direct mode" and "grid mode" calculations until all values were converged. Table S1 lists all stellar properties of the sample.

To rule out contamination from blends, we examined *TESS* pixel data and also cross-matched with the Gaia DR2 catalogue. We were able to rule out contamination within 21 arcsec down to a magnitude difference of 9 magnitudes in Gaia G band, except for four targets that appear to be resolved binaries in the Gaia catalogue.

3 High-Resolution Spectroscopy

We obtained optical high-dispersion spectra of nine stars in the sample in April and May 2019 using the HIRES spectrograph[10] at the Keck-I 10-m telescope on Maunakea observatory, Hawai'i. The spectra were obtained and reduced as part of the California Planet Search queue[11]. We typically obtained 1-minute integrations using the C5 decker, resulting in a S/N per pixel of 50 at $\sim$600 nm

with a spectral resolution of $R \sim 60000$.

High-resolution spectra for six stars were obtained in May and June 2019 using the NRES spectrograph[12] at the Las Cumbres Observatory Global Telescope Network[13] 1-meter telescopes at Cerro Tololo Inter-American Observatory, Chile and Sutherland (South Africa). Exposure times were typically 10 minutes, resulting in a S/N per resolution element above 70 at ~ 510 nm, with a spectral resolution of $R \sim 50000$.

Figure S1 shows a small region of each spectrum, alongside the Fourier amplitude spectrum. The spectral analysis was performed using the UCLSYN spectral synthesis package[14,15] using ATLAS9 models without convective overshooting[16]. Atomic data used in the analysis was obtained from the VALD database[17], using their default search and extraction parameters. Surface gravities were fixed to $\log g = 4.0$ for all stars in the analysis. A microturbulence value of 3 km s^{-1} was assumed, which is the typical value for stars within the spectral range considered here[18,19]. Measurements of the projected equatorial rotation velocity ($v \sin i$) were obtained using spectral synthesis. Individual fits to several small (5 nm) regions between 500 nm and 550 nm, avoiding any inter-order gaps, were performed to obtain values for these parameters. The final values are the mean and sample deviation of the values obtained in the small spectral regions.

Barycentric radial velocities were calculated using the Python implementation `barycorrPy`[20] of the barycentric correction algorithm of Wright et al. (2014)[21]. Space motions were calculated from *Gaia* DR2 astrometry and radial velocities and Bayesian posterior probabilities of membership in known nearby moving groups were calculated using `Banyan` Σ[22].

4 Stellar Models

The stellar models presented in Fig. 2 used the 'astero' extension of MESA (Modules for Experiments in Stellar Astrophysics)[23]. We used two approaches that gave similar results. One was based on a model grid calculated with MESA (v8118), where we varied mass (0.80–1.90 $M_\odot$ in steps of 0.01 $M_\odot$) and metallicity ([Fe/H] from -0.5 to 0.5 in steps of 0.1). We used a fixed (solar-calibrated) mixing-length parameter of $\alpha_{\rm MLT}$ = 1.9 and a helium-to-heavy-element enrichment ratio of 1.33. The best-fitting model was found by Maximum Likelihood Estimation, where we included effective temperature, metallicity, luminosity and all identified pulsation frequencies. Equal weight was given in the likelihood function to the following five observables: frequencies of radial modes, frequencies of dipolar modes, effective temperature, metallicity and luminosity. The other approach used the automated simplex search in MESA-astero (v7503), where the fit was guided by the observed radial modes only. The search was allowed to vary the mass, metallicity, mixing length, and the age of the model in order to converge to the best fit. A helium-to-heavy-element enrichment ratio of 1.4 was used. Both approaches assumed a primordial helium abundance of 0.249.

For Fig. 3a we used the evolutionary tracks with solar metallicity ($X = 0.71$, $Z = 0.014$) from Murphy et al. (2019)[24]. The other parameters of those tracks are $\alpha_{\rm MLT} = 1.8$, exponential core overshooting of 0.015 H_p (pressure scale heights), exponential H-burning shell over- and undershooting of 0.015 H_p, exponential envelope overshooting of 0.025 H_p, diffusive mixing $\log D_{\rm mix} = 0$ (in cm^{2}s^1), OPAL opacities, and the [25] solar abundance mixture. As noted by

Murphy et al. (2019), these tracks are in good agreement with the MIST tracks computed with no rotation and similar metallicities, except that the former have a longer main-sequence phase. This is not expected to be important for our targets, which are mostly young (close to the ZAMS). Although it is possible for δ Scuti pulsations to occur in the pre-main-sequence (PMS) phase, prior to the onset of hydrogen burning[26], there is no indication of a PMS classification for most of the stars in our sample.

Table S1 | Properties of high-frequency δ Scuti stars. References indicate classifications as δ Scuti stars [27–33] and λ Boo stars[34,35]. (not finished)

TIC	HD	Name	V	$T_{\rm eff}$ (K)	[Fe/H]	$v \sin i$ (km s^{-1})	$\Delta\nu$ (d^{-1})	ϵ	Refs.
589826	30422	EX Eri	6.18			128[36]	6.52	1.86	[27,35]
9147509	25369		9.68				6.15	1.65	
11199304	290750		9.77				5.96	1.49	
11361473	290799	V1790 Ori	10.67				7.55	1.65	[35,37]
24344701	34282	V1366 Ori	9.92			129[38]	7.40	1.71	[31]
31475829	37286	HR 1915	6.26			70[39]	7.30	—	[39,40]
32763133	38629		8.92				7.35	1.77	[28]
34197596	25674		8.69				6.75	1.79	[28]
34737955	44930		9.42				6.03	1.67	[34]
37498433	42608		9.85			41	7.10	1.57	[28]
43363194	3622		7.77			50	6.89	1.61	
44645679	24975		7.24				6.23	1.58	
71134596	28548		9.22				7.50	1.67	[28,34]
78492107	50153		7.03				6.85	1.60	
100531058	38597		8.65				6.90	1.68	[28]
112484997	59594	V349 Pup	7.32				6.65	1.61	[27]
117766204	45424		7.18				6.54	1.86	
122615966	17341		9.32				5.90	1.73	[34]
122686610	17693		7.80				6.41	1.61	
124381332		TYC 5945-497-1	9.69			178	7.45	1.61	[28]
124429243	42915		9.04			118	6.40	1.98	[28]
143381070		SAO 150524	9.46				7.63	—	
148228220	48985		9.04				7.25	1.56	
150272131	44726		10.38				7.25	1.70	[28]
159895674	20232		6.88				6.86	1.64	
172193026	46722		9.29				6.45	1.71	[34]
176400189	75040		9.05			24	6.64	1.58	
224284988	223011		6.32			43	5.93	1.68	
229139161	10779		8.78				6.80	1.63	
231014033	10961		9.39				7.30	1.70	
242944780	24572		9.45				7.20	1.58	[28]
246902545	31322		9.28				6.10	1.69	[28]
255548143	44958	V435 Car	6.74			114	6.90	1.58	[27]
259675399	31640		8.06				6.41	1.75	
260161111		TYC 8533-329-1	10.70				7.27	—	[28]
269792989	29783		7.87				6.74	1.79	
270577175	39060	β Pic	3.85			122[41]	6.95	—	[32,33]

TIC	HD	Name	V	$T_{\rm eff}$ (K)	[Fe/H]	$v \sin i$ (km s^{-1})	$\Delta\nu$ (d^{-1})	ϵ	Refs.
274038922	20203		8.85				7.20	1.76	[28]
278179191	59104		8.50				6.96	1.67	
281499618	2280		9.13				7.17	1.73	
282265535	40317		8.45				6.95	1.63	
284348793	54711		9.01				7.08	1.65	
287347434	99506		8.36			26	7.05	1.59	
294157254	55863		9.06				6.92	1.57	
306773428	67688		7.66				7.04	1.59	
316806320	222496		9.48				5.63	1.71	
316920092	31901		9.07				6.97	1.56	
327996759	220811		6.91			273	6.04	1.82	
332516661	78198		9.50			45	5.90	1.65	
340358522		TYC 8564-537-1	10.59				7.15	1.54	
348792358	32433		9.22				6.95	1.54	
349645354		SAO 249859	9.79				5.34	1.69	
388351327	70510		6.75			94	7.16	1.68	
408906554	42005		9.54				7.16	1.57	[28]
431695696		TYC 85-867-1	9.63				7.26	1.61	
459942890	25248		8.60				7.16	1.55	
463556278	89263	HR 4043	6.22			100	7.02	1.71	
KIC 7548479	187547		8.40			10^{29}	7.00	1.61	[29,30]
KIC 8415752		TYC 3132-1272-1	10.67			18	6.20	1.63	
KIC 9450940			12.68			10	6.15	1.67	

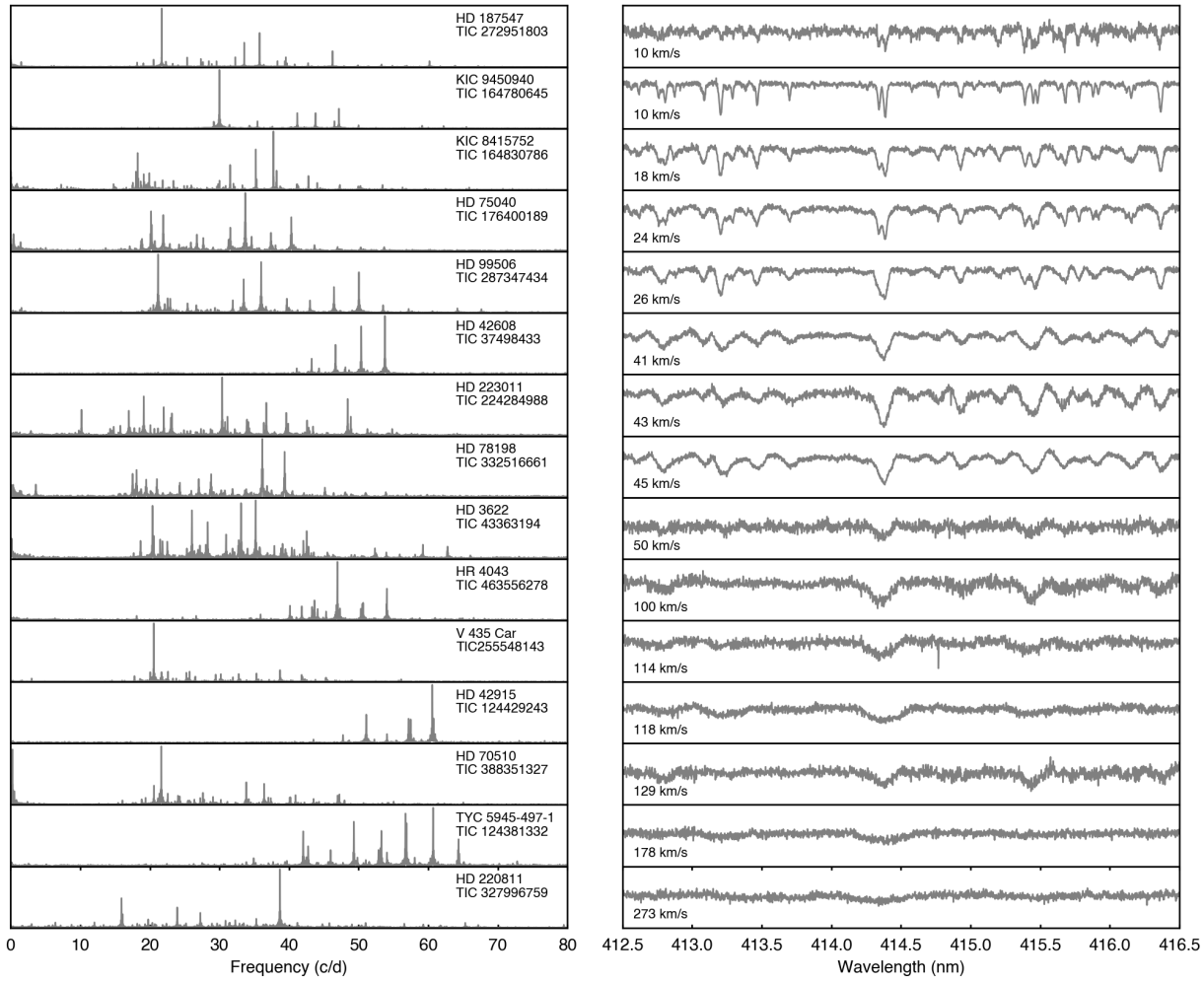

Figure S1 | Fourier amplitude spectra and high-resolution spectra of high-frequency δ Scuti stars. Measured $v \sin i$ values are shown in the right panel and the stars are sorted by increasing $v \sin i$.

5 Notes on individual stars

- HD 187547 (KIC 7548479): the large frequency spacing was previously reported as 40.5 μHz (3.5 d^{-1})[29,30], which is factor of two smaller than the value we have identified from the same *Kepler* observations.

- HD 34282 (V1366 Ori): based on observations with MOST, Casey et al. (2013)[31] reported a large separation of 3.75 d^{-1}, which is half the value reported here.

- β Pic: known to be a high-frequency δ Scuti star[32,33], but a value for the large separation has not been reported.

- EX Eri (HD 30422, HIP 22192): this is a λ Boo star[35] that was catalogued as a high-frequency δ Scuti pulsator[27], and which has an infrared excess consistent with a debris disk[42].

The following stars are not in our sample but seem likely to be high-frequency δ Scuti stars with regular spacings:

- HD 144277: based on MOST and CoRoT data, Zwintz et al. (2011)[43] suggested a large separation of 7.2 d^{-1}. This star will not be observed by *TESS* in its nominal two-year mission (ecliptic latitude $-18.0°$).

- HD 261711: based on MOST and CoRoT data, Zwintz et al. (2013)[44] suggested a large separation of 6.72 d^{-1}. This star was observed by *TESS* in Sector 6, but only in long-cadence mode.

References

1. Høg, E. *et al.* The Tycho-2 catalogue of the 2.5 million brightest stars. *Astron. Astrophys.* **355**, L27–L30 (2000).

2. Bessell, M. S. The Hipparcos and Tycho Photometric System Passbands. *Pub. Astron. Soc. Pac.* **112**, 961–965 (2000).

3. Flower, P. J. Transformations from Theoretical Hertzsprung-Russell Diagrams to Color-Magnitude Diagrams: Effective Temperatures, B-V Colors, and Bolometric Corrections. *Astrophys. J.* **469**, 355 (1996).

4. Lindegren, L. *et al.* Gaia Data Release 2. The astrometric solution. *Astron. Astrophys.* **616**, A2 (2018).

5. Bovy, J., Rix, H.-W., Green, G. M., Schlafly, E. F. & Finkbeiner, D. P. On Galactic Density Modeling in the Presence of Dust Extinction. *Astrophys. J.* **818**, 130 (2016).

6. Huber, D. *et al.* The K2 Ecliptic Plane Input Catalog (EPIC) and Stellar Classifications of 138,600 Targets in Campaigns 1-8. *Astrophys. J.* **224**, 2 (2017).

7. Choi, J. *et al.* Mesa Isochrones and Stellar Tracks (MIST). I. Solar-scaled Models. *Astrophys. J.* **823**, 102 (2016).

8. Casagrande, L. *et al.* New constraints on the chemical evolution of the solar neighbourhood and Galactic disc(s). Improved astrophysical parameters for the Geneva-Copenhagen Survey. *Astron. Astrophys.* **530**, A138 (2011).

9. Mathur, S. *et al.* Revised Stellar Properties of Kepler Targets for the Q1-17 (DR25) Transit Detection Run. *Astrophys. J. Suppl. Ser.* **229**, 30 (Erratum: ApJS, 234, 43) (2017).

10. Vogt, S. S. *et al.* HIRES: the high-resolution echelle spectrometer on the Keck 10-m Telescope. In Crawford, D. L. & Craine, E. R. (eds.) *Society of Photo-Optical Instrumentation Engineers (SPIE) Conference Series*, vol. 2198 of *Society of Photo-Optical Instrumentation Engineers (SPIE) Conference Series*, 362 (1994).

11. Howard, A. W. *et al.* The California Planet Survey. I. Four New Giant Exoplanets. *Astrophys. J.* **721**, 1467–1481 (2010).

12. Siverd, R. J. *et al.* NRES: the network of robotic echelle spectrographs. In *Ground-based and Airborne Instrumentation for Astronomy VII*, vol. 10702 of *Society of Photo-Optical Instrumentation Engineers (SPIE) Conference Series*, 107026C (2018).

13. Brown, T. M. *et al.* Las Cumbres Observatory Global Telescope Network. *Pub. Astron. Soc. Pac.* **125**, 1031 (2013).

14. Smith, K. C. & Dworetsky, M. M. Report for Workshop on Elemental Abundances Analyses. In Adelman, S. J. & Lanz, T. (eds.) *Elemental Abundance Analyses*, 32 (1988).

15. Smith, K. C. *The chemical compositions of mercury-manganese stars from ultraviolet spectra*. Ph.D. thesis, University of London, University College London (United Kingdom (1992).

16. Castelli, F., Gratton, R. G. & Kurucz, R. L. Notes on the convection in the ATLAS9 model atmospheres. *Astron. Astrophys.* **318**, 841–869 (1997).

17. Kupka, F., Piskunov, N., Ryabchikova, T. A., Stempels, H. C. & Weiss, W. W. VALD-2: Progress of the Vienna Atomic Line Data Base. *Astron. Astrophys. Suppl. Ser.* **138**, 119–133 (1999).

18. Niemczura, E. *et al.* Spectroscopic survey of Kepler stars. I. HERMES/Mercator observations of A- and F-type stars. *Mon. Not. R. Astron. Soc.* **450**, 2764–2783 (2015).

19. Niemczura, E. *et al.* Spectroscopic survey of Kepler stars - II. FIES/NOT observations of A- and F-type stars. *Mon. Not. R. Astron. Soc.* **470**, 2870–2889 (2017).

20. Kanodia, S. & Wright, J. Python leap second management and implementation of precise barycentric correction (barycorrpy). *Research Notes of the AAS* **2**, 4 (2018).

21. Wright, J. T. & Eastman, J. D. Barycentric Corrections at 1 cm s^{-1} for Precise Doppler Velocities. *Pub. Astron. Soc. Pac.* **126**, 838 (2014).

22. Gagné, J. *et al.* BANYAN. XI. The BANYAN Σ Multivariate Bayesian Algorithm to Identify Members of Young Associations with 150 pc. *Astrophys. J.* **856**, 23 (2018).

23. Paxton, B. *et al.* Modules for Experiments in Stellar Astrophysics (MESA): Planets, Oscillations, Rotation, and Massive Stars. *Astrophys. J. Suppl. Ser.* **208**, 4 (2013).

24. Murphy, S. J., Hey, D., Van Reeth, T. & Bedding, T. R. Gaia-derived luminosities of Kepler A/F stars and the pulsator fraction across the δ Scuti instability strip. *Mon. Not. R. Astron. Soc.* **485**, 2380–2400 (2019).

25. Asplund, M., Grevesse, N., Sauval, A. J. & Scott, P. The Chemical Composition of the Sun. *Ann. Rev. Astron. Astrophys.* **47**, 481–522 (2009).

26. Zwintz, K. *et al.* Echography of young stars reveals their evolution. *Science* **345**, 550–553 (2014).

27. Rodríguez, E., López-González, M. J. & López de Coca, P. A revised catalogue of delta Sct stars. *Astron. Astrophys. Suppl. Ser.* **144**, 469–474 (2000).

28. Holdsworth, D. L. *et al.* High-frequency A-type pulsators discovered using SuperWASP. *Mon. Not. R. Astron. Soc.* **439**, 2078–2095 (2014).

29. Antoci, V. *et al.* The excitation of solar-like oscillations in a δSct star by efficient envelope convection. *Nature* **477**, 570–573 (2011).

30. Antoci, V. *et al.* The Role of Turbulent Pressure as a Coherent Pulsational Driving Mechanism: The Case of the δ Scuti Star HD 187547. *Astrophys. J.* **796**, 118 (2014).

31. Casey, M. P. *et al.* MOST observations of the Herbig Ae δ-Scuti star HD 34282. *Mon. Not. R. Astron. Soc.* **428**, 2596–2604 (2013).

32. Mékarnia, D. *et al.* The δ Scuti pulsations of β Pictoris as observed by ASTEP from Antarctica. *Astron. Astrophys.* **608**, L6 (2017).

33. Zwintz, K. *et al.* Revisiting the pulsational characteristics of the exoplanet host star β Pictoris. *arXiv e-prints* arXiv:1905.12545 (2019).

34. Gray, R. O. *et al.* The Discovery of λ Bootis Stars: The Southern Survey I. *Astron. J.* **154**, 31 (2017).

35. Murphy, S. J. *et al.* An Evaluation of the Membership Probability of 212 λ Boo Stars. I. A Catalogue. *Pub. Astron. Soc. Aust.* **32**, e036 (2015).

36. Royer, F., Zorec, J. & Gómez, A. E. Rotational velocities of A-type stars. III. Velocity distributions. *Astron. Astrophys.* **463**, 671–682 (2007).

37. Paunzen, E. *et al.* λ Bootis stars in the SuperWASP survey. *Mon. Not. R. Astron. Soc.* **453**, 1241–1248 (2015).

38. Mora, A. *et al.* EXPORT: Spectral classification and projected rotational velocities of Vega-type and pre-main sequence stars. *Astron. Astrophys.* **378**, 116–131 (2001).

39. Royer, F., Grenier, S., Baylac, M. O., Gómez, A. E. & Zorec, J. Rotational velocities of A-type stars in the northern hemisphere. II. Measurement of v sin i. *Astron. Astrophys.* **393**, 897–911 (2002).

40. Zuckerman, B., Rhee, J. H., Song, I. & Bessell, M. S. The Tucana/Horologium, Columba, AB Doradus, and Argus Associations: New Members and Dusty Debris Disks. *Astrophys. J.* **732**, 61 (2011).

41. Schröder, C., Reiners, A. & Schmitt, J. H. M. M. Ca II HK emission in rapidly rotating stars. Evidence for an onset of the solar-type dynamo. *Astron. Astrophys.* **493**, 1099–1107 (2009).

42. Morales, F. Y., Bryden, G., Werner, M. W. & Stapelfeldt, K. R. Herschel-resolved Outer Belts of Two-belt Debris Disks—Evidence of Icy Grains. *Astrophys. J.* **831**, 97 (2016).

43. Zwintz, K. *et al.* Regular frequency patterns in the classical δ Scuti star HD 144277 observed by the MOST satellite. *Astron. Astrophys.* **533**, A133 (2011).

44. Zwintz, K. *et al.* Regular frequency patterns in the young δ Scuti star HD 261711 observed by the CoRoT and MOST satellites. *Astron. Astrophys.* **552**, A68 (2013).